Formation of ozone: Metastable states and anomalous isotope effect

Dmitri Babikov,[a] Brian K. Kendrick, Robert B. Walker, and Russell T Pack
Theoretical Division, Los Alamos National Laboratory, Los Alamos, New Mexico 87545

Paul Fleurat-Lesard and Reinhard Schinke
Max-Planck-Institute für Strömungsforschung, D-37073 Göttingen, Germany

(Received 24 April 2003; accepted 7 May 2003)

A clear explanation for an anomalous isotope effect in ozone formation is given in terms of the energy transfer mechanism, where the metastable states of ozone are formed first, and then stabilized by collisions with other atoms. Unusual nonstatistical properties of metastable states spectra discovered earlier [J. Chem. Phys. **118**, 6298 (2003)] are incorporated into the kinetics model, where different metastable states are treated as different species, and the stabilization step is treated approximately. The population of the ozone metastable states builds up and decays through three possible O_2+O channels. When different isotopes of oxygen are involved the three channels become open at different energies because of the differences in the quantum zero-point-energies (ΔZPE) of the different O_2 molecules. The spectrum of metastable states is anomalously dense below the ΔZPE threshold and these states are accessible only from the lower entrance channel. Also, these low-lying metastable states are stabilized very efficiently (by collisions with third body) because they are energetically close to the bound O_3 states. Such processes significantly enhance the formation rates of ozone isotopologues through the lower channels over the formation rates through the upper channels. Numerical results obtained for $J=0$ give isotope effects in the right direction and of the right order of magnitude. Consideration of $J>0$ should improve the comparison with experiment. © *2003 American Institute of Physics*. [DOI: 10.1063/1.1587113]

I. INTRODUCTION

Ozone is a very important component of earth's atmosphere. In the lower atmosphere (troposphere) ozone is a destructive pollutant formed in man-caused smog and is a problem for many industrial cities. But in the upper atmosphere (stratosphere) ozone is essential in protecting life on earth from dangerous ultraviolet radiation from the sun. We must preserve stratospheric ozone (keep the "ozone hole" from getting any deeper) and, at the same time, reduce man-caused tropospheric ozone.

Oxygen has three stable isotopes: ^{16}O, ^{17}O, and ^{18}O. The isotope ^{16}O is dominant in the atmosphere, so that most oxygen molecules (O_2) only include ^{16}O atoms. However, it has been known for more then 20 years now that, as first reported[1] in 1981, stratospheric ozone (O_3) shows strange, large enrichments in the heavy isotopes of oxygen relative to the oxygen from which it is formed. In 1983 anomalous large enrichment was confirmed by the laboratory studies[2] as well and it was shown to be "*mass independent*," i.e., almost equal for ^{17}O and ^{18}O. For recent short reviews, see Thiemens[3] and Mauersberger *et al.*[4]

Explaining the anomalous isotope effect for ozone formation will have a significant impact on improving our understanding of ozone's chemistry, production, lifetime, and loss in the atmosphere. It will allow the isotopic composition of O_3 to be used as a reliable probe of its source and history for studying atmospheric chemistry, global climate change, atmospheres of other planets, and the history of the solar system.[3] Similar anomalous isotope effects are found in stratospheric versus tropospheric CO_2, N_2O, and CO, and the enrichment in these molecules is believed to be a consequence of subsequent reactions with the enriched O_3 present.[5] Understanding O_3 enrichment will provide the key to understanding it for other molecules. Even without being understood, the isotopic composition of CO_2 in the atmosphere is already being used[3] as a probe to identify its source, and it influences models aimed at studying the global carbon budget.

At first, it was not at all clear which step in the atmospheric ozone cycle was isotopically selective, but careful experimental work[6] traced it clearly to the recombination reaction which forms ozone,

$$O+O_2+M \Rightarrow O_3+M. \quad (1)$$

Here the third body M may be any atmospheric atom or molecule, O_3 may be formed as any combination of ^{16}O, ^{17}O and ^{18}O isotopes. In the laboratory experiments Mauersberger and co-workers[3,7–11] have measured the rate coefficients for reaction (1) for many of the possible isotopic combinations of reactants O and O_2 and can derive from them the rates of many other combinations. Their results show that the rates *do* depend on the masses of the oxygen atoms involved, and for different isotopic compositions the rates can differ by more then 50%, which is a remarkably large isotope effect! The dependence on mass is, nevertheless, very complex.

The isotope effect in reaction (1) is essentially independent[12,13] of the identity of the third body M, and oc-

[a]Author to whom all correspondence should be addressed; electronic mail: babikov@lanl.gov

curs with M being as simple as Ar or He. For these, the reaction mechanism at low pressure is expected to be dominated by the *energy transfer* (ET) mechanism:

$$O + O_2 \Leftrightarrow O_3^*, \tag{2}$$

$$O_3^* + M \Rightarrow O_3 + M. \tag{3}$$

Here O_3^* is a metastable state (or scattering resonance) which lives long enough to be stabilized by the collision with M. Again, any combination of O isotopes can be involved.

Early theoretical attempts to explain these effects have not had much success. The first attempts[14] predicted *depletion* where *enrichment* was actually observed! Classical trajectory simulations have been performed,[15] but these give a tiny isotope effect in the *opposite* direction from experiment. Bates published a series of seven papers spread over seven years attempting to explain it. He noted that unsymmetric molecules, such as $^{18}O\,^{16}O\,^{16}O$, where the heavy atom is on the end of the ozone (O_3 is a bent triatomic), are enriched much more than the symmetric isotopomer, such as $^{16}O\,^{18}O\,^{16}O$, where the heavy atom is in the middle. The first explanations he proposed were later shown to be nothing more than the rotational symmetry numbers that have been known from statistical mechanics for over 60 years. Experimentalists had already accounted for them in reporting their results. Later, in his most detailed work,[16] he treated reaction (1) as proceeding via the ET mechanism, and he allowed for symmetry in calculating the concentration of metastable intermediate O_3^*. However, he took the rate of deactivation to be the same for all isotopic combinations, not recognizing that unsymmetric molecules not only have more states but also more relaxation pathways. His results explained a few experiments but failed on many others.

Gellene[17] has given a model of symmetry induced kinetic isotope effects (SIKIE) that works quite well on some ion–molecule reactions but fails on rates for reaction (1). Clearly, from the experimental results, symmetry is playing a very important role, but the whole effect is far more complicated than that. If symmetry were dominant, then the reactions $^{18}O + ^{16}O\,^{16}O \rightarrow ^{18}O\,^{16}O\,^{16}O$ and $^{16}O + ^{18}O\,^{18}O \rightarrow ^{16}O\,^{18}O\,^{18}O$, which have the same symmetry, should have the same rates. However, the first is the *slowest* of all the possible combinations, while the second is the *fastest*.[9] Hence, mass also plays a huge role, and experimental results illustrate that attack by the lighter atoms tends to give the larger rates.

However, recent work is tantalizing. Charlo and Clary[18] performed approximate quantum calculations (reduced dimensionality+sudden approximation) of the recombination rate and found isotopic effects of the right order of magnitude but often in the wrong direction. Miklavc and Peyerimhoff[19] showed that a crude model for the vibrational excitation of O_2 by O gave probabilities in the same ratios as the recombination rates. Gellene[20] used analysis of classical trajectories to get insight into the mechanism of formation of the metastable ozone states. Independently of each other and at almost the same time the groups of Mauersberger at Heidelberg and Marcus at Cal Tech have emphasized the importance of the quantum zero-point energies (ZPE) of O_2 reactants/products for the isotope effect. Mauersberger and co-workers found[9,10,21] that the formation rates for different isotopic compositions of ozone correlate *not with the masses* of the oxygen atoms involved, but with *the ZPE change* (ΔZPE) of the O_2 molecule in the corresponding atom exchange reaction:

$$^xO + ^yO\,^zO \Leftrightarrow (^xO\,^yO\,^zO)^* \Leftrightarrow ^xO\,^yO + ^zO. \tag{4}$$

Here, the metastable state $(^xO\,^yO\,^zO)^*$ can be formed from both sides of this reaction and can decay either to the right or left. Reaction (2) is part of this reaction. When different isotopes of oxygen (x, y, and z) are involved, the ZPE of the O_2 molecules on the right- and left-hand sides may be different, and reaction (4) can thus be slightly exothermic or slightly endothermic. Mauersberger and co-workers[21] propose to correlate endothermic exchange reactions with longer lifetimes of the metastable O_3^* formed, and exothermic exchange reactions with shorter lifetimes. They expect that longer lifetimes of O_3^* increase the probability of its stabilization into bound O_3 by a collision with another body M. For ozone the reaction (4) is about 2000 times faster than reaction (3),[21] so that atom exchange quickly reshuffles various oxygen isotopes available in the mixture and achieves equilibrium between the various O, O_2, and O_3^* species present before the stabilizing collision with M occurs. Thus, their idea is that the *lifetimes* of the metastable states O_3^* with different isotopic compositions define the formation rates of O_3. We found this idea very attractive, because resonances are known to be very sensitive to the masses of atoms involved. In this paper we shall show that Mauersberger and co-workers have come very close to the resolution of the problem; however, they had no direct experimental way to measure the metastable states involved in reaction (3) and their dependence on ΔZPE. It is clear that accurate quantum mechanical calculations of positions and lifetimes of the metastable states O_3^* are required.

Alternatively, Marcus and co-workers[22–28] have used a statistical (RRKM)-based theory to treat the recombination. They emphasized importance of two effects for explanation of ozone formation anomalies. The *first* of these is an empirical *nonstatistical* factor (η parameter) to describe a difference in density of dynamically active O_3^* states in symmetric and nonsymmetric ozone molecules. They demonstrated that this η effect is dominant in determining the anomalous mass-independent isotope enrichments in stratospheric conditions. The *second* factor is necessary to explain the mass-dependence observed in the recombination rates. This is a ''partitioning factor'' that depends on the ''differences in zero-point energies of the two transition states'' in reaction (2) that connect with isotopically different O_2 molecules. Tuning these and other parameters to fit the experimental data for two extreme cases (the slowest $^{18}O + ^{16}O\,^{16}O \rightarrow ^{18}O\,^{16}O\,^{16}O$ and the fastest $^{16}O + ^{18}O\,^{18}O \rightarrow ^{16}O\,^{18}O\,^{18}O$) allowed them to reproduce the experimental data for other isotopic combinations quite well. They have come very close to a solution of the problem, but their factors are empirical parameters that do not follow from their theory. Finally, they have also recognized[24,25] that rigorous

detailed quantum mechanical calculations for various isotopologues of ozone are needed in order to accurately describe the isotope effects.

Recently, we have reported[29] such a rigorous theoretical study: the first full quantum mechanical calculations of the three-body resonances for three isotopologues of ozone: $^{16}O\,^{16}O\,^{16}O$, $^{16}O\,^{18}O\,^{18}O$, and $^{18}O\,^{16}O\,^{16}O$. We have discovered a strong nonstatistical feature of O_3^* lifetime spectrum and explained it by the difference in ZPE of two formation/decay channels. Also, in a brief communication[30] we have qualitatively shown that this feature is responsible for the anomalous rates of ozone formation. In the present paper we give a quantitative treatment of ozone formation kinetics based on our resonance spectra and describe quantitatively the ΔZPE effect on recombination rates.

II. KINETICS OF OZONE FORMATION

In our treatment of ozone formation kinetics we will consider different metastable $O_3^*(E_i)$ states as different species.[31] Here E_i is the energy of the ith metastable state and the index i labels the metastable states. The total concentration of the metastable complexes $[O_3^*]$ is a sum of concentrations of all states:

$$[O_3^*]=\sum_i [O_3^*(E_i)]. \tag{5}$$

We will consider the general form of Eq. (4), where we label two possible channels of ozone formation as A and B:

$$^{B}O+{}^{B}O_2 \underset{k_i^{d_B}}{\overset{k_i^{f_B}}{\rightleftarrows}} O_3^*(E_i) \underset{k_i^{f_A}}{\overset{k_i^{d_A}}{\rightleftarrows}} {}^{A}O+{}^{A}O_2. \tag{6}$$

Here we have introduced the channel-specific reactants/products ($^{A}O+{}^{A}O_2$ and $^{B}O+{}^{B}O_2$) and channel-specific rate coefficients for formation ($k_i^{f_A}$ and $k_i^{f_B}$) and dissociation ($k_i^{d_A}$ and $k_i^{d_B}$) of the metastable $O_3^*(E_i)$ states. For the stabilization step of the $O_3^*(E_i)$ state we have

$$O_3^*(E_i)+M \overset{k_i^s}{\rightarrow} O_3+M, \tag{7}$$

where the second-order stabilization rate coefficient k_i^s for each metastable state is introduced as

$$\frac{d[O_3]}{dt}=\sum_i k_i^s[O_3^*(E_i)][M]. \tag{8}$$

The master equation for the concentration of the metastable states is then [see Eqs. (6) and (7)]:

$$\frac{d[O_3^*(E_i)]}{dt}=k_i^{f_A}[{}^{A}O][{}^{A}O_2]+k_i^{f_B}[{}^{B}O][{}^{B}O_2]-k_i^{d_A}[O_3^*(E_i)] - k_i^{d_B}[O_3^*(E_i)]-k_i^s[O_3^*(E_i)][M]. \tag{9}$$

Assuming the steady state conditions:

$$\frac{d[O_3^*(E_i)]}{dt}\approx 0, \tag{10}$$

we obtain from Eq. (9) for the concentration of the metastable states:

$$[O_3^*(E_i)]=\frac{k_i^{f_A}[{}^{A}O][{}^{A}O_2]+k_i^{f_B}[{}^{B}O][{}^{B}O_2]}{k_i^{d_A}+k_i^{d_B}+k_i^s[M]}. \tag{11}$$

Here, the channel-specific rates of $O_3^*(E_i)$ formation can be expressed using channel-specific equilibrium constants:

$$k_i^{f_A}=k_i^{d_A}K_i^A, \quad k_i^{f_B}=k_i^{d_B}K_i^B. \tag{12}$$

Substitution of Eq. (12) into Eq. (11) and following substitution of the result into Eq. (8) give us

$$\frac{d[O_3]}{dt}=[{}^{A}O_2][{}^{A}O][M]\sum_i \frac{k_i^{d_A}K_i^A k_i^s}{k_i^{d_A}+k_i^{d_B}+k_i^s[M]} + [{}^{B}O_2][{}^{B}O][M]\sum_i \frac{k_i^{d_B}K_i^B k_i^s}{k_i^{d_A}+k_i^{d_B}+k_i^s[M]}. \tag{13}$$

The channel-specific third-order recombination rate coefficients (κ^A and κ^B) can be introduced as

$$\frac{d[O_3]}{dt}=\left.\frac{d[O_3]}{dt}\right|_A+\left.\frac{d[O_3]}{dt}\right|_B =[{}^{A}O_2][{}^{A}O][M]\kappa^A+[{}^{B}O_2][{}^{B}O][M]\kappa^B. \tag{14}$$

Here the two terms represent the change in time of O_3 concentration via channels A and B, respectively. Comparing expressions (13) and (14) we obtain for channel A:

$$\kappa^A=\sum_i \kappa_i^A, \tag{15}$$

$$\kappa_i^A=\frac{k_i^{d_A}}{k_i^{d_A}+k_i^{d_B}+k_i^s[M]}K_i^A k_i^s. \tag{16}$$

Similarly, for channel B we obtain

$$\kappa^B=\sum_i \kappa_i^B, \tag{17}$$

$$\kappa_i^B=\frac{k_i^{d_B}}{k_i^{d_A}+k_i^{d_B}+k_i^s[M]}K_i^B k_i^s. \tag{18}$$

Equations (16) and (18) for channel-specific recombination rate coefficients are the final results of this section. Equations (15) and (17) show that the total recombination rate coefficient is just a sum of contributions from all metastable states $O_3^*(E_i)$.

When the energy E_i is low enough that only one formation/dissociation channel is open, we have from Eq. (16) or (18):

$$\kappa_i=\frac{k_i^d}{k_i^d+k_i^s[M]}K_i k_i^s, \tag{19}$$

where k_i^d is a rate coefficient for decay of $O_3^*(E_i)$ via that channel. In the low pressure limit ($k_i^d \gg k_i^s[M]$) this gives the well-known result for the recombination rate coefficient: $\kappa_i = K_i k_i^s$.

The channel-specific equilibrium constants K_i^A and K_i^B for Eqs. (16) and (18) are obtained by counting calculated quantum states of diatomic O_2 reactants/products and of metastable $O_3^*(E_i)$ intermediates:

$$K_i^A = \frac{Q_{O_3^*(E_i)}}{Q_{^AO} Q_{^AO_2}} = \frac{(2J+1)^2 \exp\left\{-\frac{E_i}{kT}\right\}}{g_e(T)\left(\frac{\mu_A kT}{2\pi\hbar^2}\right)^{3/2} \sum_{j_A} (2j_A+1)\exp\left\{-\frac{\varepsilon_{j_A}}{kT}\right\}}. \quad (20)$$

Here J is the total angular momentum quantum number for the $O_3^*(E_i)$ metastable state, j_A is rotational quantum number for channel diatomic $^AO_2$ (including symmetry restrictions), and ε_{j_A} is the corresponding eigenvalue, μ_A is a channel-specific reduced mass of the O_2+O pair, and g_e is the electronic partition function of $O_2(^3\Sigma_g)+O(^3P_2)$.[20,23] In Eq. (20) we keep only the first term of the vibrational partition function for O_2 which corresponds to the ground vibrational state $v=0$ of diatomic reactants/products. This is justified at room temperature and below when all $v>0$ terms in the partition function are negligibly small.

The final step of ozone formation—stabilization of the metastable states [Eq. (7)]—is treated only approximately here, as has often been done in other studies.[20,23] (In subsequent papers we plan a more accurate treatment.) We adopt the "*exponential down*" model[32] and calculate stabilization rate coefficients needed in Eqs. (16) and (18) simply as

$$k_i^s = \beta(E_i)\omega(T). \quad (21)$$

Here ω is Lenard-Jones collision frequency for stabilizing O_3^*+M collisions[23] and β is exponential stabilization probability:[32]

$$\beta(E_i) = \exp\{-E_i/\Delta E\}. \quad (22)$$

A small value of $\Delta E = 35\ cm^{-1}$ was taken in accordance with recent classical trajectory studies[20] and available experimental information.[33]

However, the crucial step of the recombination process—formation and decay of the metastable states [Eq. (6)]—is treated in a very sophisticated way using full quantum mechanics to determine energies and lifetimes of the metastable $O_3^*(E_i)$ states and related rate coefficients $k_i^{d_A}$ and $k_i^{d_B}$ needed for Eqs. (16) and (18).

III. LIFETIMES OF THE METASTABLE STATES

As discussed in our earlier papers,[29,30] a very sophisticated potential energy surface (PES) for ozone was used for this work. It is based on an accurate *ab initio* calculations[34,35] and includes a correction in the barrier region to make it agree with even more accurate *ab initio* calculations performed along the minimum energy path.[36] It is the most accurate PES currently available for the ground electronic state of ozone. It has the full symmetry of the system and goes smoothly to all the correct dissociation limits. It exhibits a small barrier along the dissociation path, but the top of that barrier is *below* the dissociation limit.

Details of the scattering calculations are given in Ref. 29 and references therein; only a brief summary is given here. We have performed full quantum reactive scattering calculations in all six dimensions of the problem (required for the triatomic ozone molecule). No approximations have been made. Energies up to 0.052 eV (~600 K) above the dissociation threshold have been studied. The present calculations have been performed for total angular momentum $J=0$; calculations for $J>0$ are ongoing and will be reported later. A coupled channel (CC) approach using APH hyperspherical coordinates and a hybrid FBR/DVR[37] is employed. The parallel computer code of Kendrick[38] was used, which provides an accurate treatment of Eckart singularities and a proper description of symmetry. Propagation of the coupled channel equations is performed using the log-derivative method.[39,40]

The lifetimes of the scattering states were obtained from the trace of the collision lifetime (**Q**) matrix:[41]

$$\mathbf{Q} \equiv i\hbar \mathbf{S} \frac{\partial \mathbf{S}^+}{\partial E}, \quad (23)$$

where **S** is the scattering matrix. The calculated lifetime spectra of the metastable states for $^{16}O\,^{16}O\,^{16}O$, $^{16}O\,^{16}O\,^{18}O$ and $^{16}O\,^{18}O\,^{18}O$ isotopologues in the low energy range ($E_i < 110$ K) were presented and discussed in our previous paper.[29] In the present paper we present the lifetime spectrum for the $^{16}O\,^{18}O\,^{18}O$ isotopologue over a wide energy range: $E_i < 600$ K (see Fig. 1). The lifetime obtained from the **Q** matrix represents the difference between the actual time required for a collision and the time that a collision would have taken if the interaction potential were zero. Both the acceleration of reactants due to the strong attractive well and the shortened path due to the repulsive potential wall can make the actual collision time significantly shorter and thus lead to a negative background lifetime. Hence, the negative background of the spectrum corresponds to the relatively fast (nonresonant) $O+O_2$ scattering or atom exchange processes, while the sharp spikes (scattering resonances) correspond to the formation of long-lived metastable O_3^* states. The spectrum is very nonstatistical: the lower narrow part of the spectrum ($E_i < 29$ K, 0.0946 eV in Fig. 1) is dense—it contains *many long-lived metastable states*, while the higher energy region of the spectrum (29 K $< E_i <$ 240 K, 0.1125 eV in Fig. 1) is *very sparse* and contains only a few resonant features (see also Fig. 5 in Ref. 29). This interesting behavior is due to the difference in ZPE of the $^{18}O\,^{18}O$ and $^{16}O\,^{18}O$ diatomics (ΔZPE).[29] The ZPE of the lighter diatomic, $^{16}O\,^{18}O$, is about 29 K higher than the ZPE of the heavier diatomic, $^{18}O\,^{18}O$, so that both $^{16}O+{}^{18}O\,^{18}O$ and $^{18}O+{}^{16}O\,^{18}O$ dissociation channels are open at energies above 29 K. Below this energy, in the ΔZPE energy range ($E_i < 29$ K), one dissociation channel ($^{18}O+{}^{16}O\,^{18}O$) is closed; this provides more favorable conditions for formation of many long-lived metastable states. At energies above the ΔZPE both dissociation channels are open, so that the metastable states decay more easily (see also the discussion in Ref. 29).

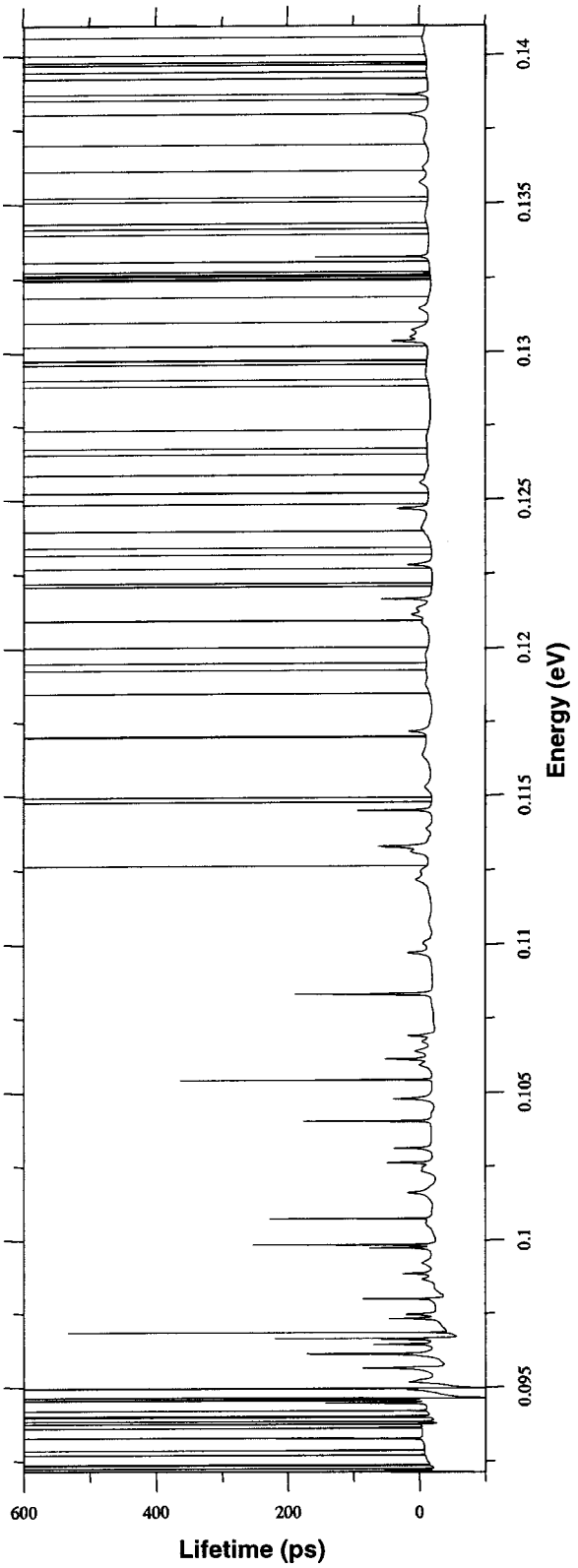

FIG. 1. Calculated lifetime spectrum for $^{16}O\,^{18}O\,^{18}O$ isotopologue. Sharp spikes to the left on the spectrum correspond to long-lived metastable states (scattering resonances). See the text for discussion.

Table I gives the positions and lifetimes of the resonances at energies $E_i<240$ K. Interpolation using a rational function was performed between calculated energy points in the vicinity of each resonance maximum and the positions E_i and lifetimes $\mathrm{Tr}\{\mathbf{Q}(T_i)\}$ of the interpolant maximum are given as the first and the second columns of the table. This procedure for locating the resonance maximum is very accurate. An approximate value of the negative nonresonant background in the region of each resonance is given in the third column. In this work we have employed a more accurate treatment of the nonresonant background than that in our previous paper; this makes the background values of several resonances in Table I here slightly different from the values reported earlier (Table I of Ref. 29). The relative lifetime τ_i (value at the maximum minus the background value) is given in column four.

New features appear in a lifetime spectrum at energies $E_i>240$ K. At these energies we have found many long-lived metastable states with lifetimes in the microsecond range! Figure 2 plots the same part of the spectrum as in Fig. 1 but on a different lifetime scale, so that the lifetimes of very long-lived resonances are easily seen. We have identified 50 such metastable states in the energy range 240 K $<E_i<600$ K. One such resonance with a lifetime $\tau_i \approx 11.28\ \mu$s is shown in Fig. 3. The origin of these very long-lived metastable states is not yet understood, but we show later in this section that they are not important for the recombination process, so we do not focus on them in the present paper.

Use of the APH hyperspherical coordinates automatically involves consideration of all possible permutations of nuclei simultaneously, so that all possible ozone equilibrium structures and all accessible ozone formation channels are taken into account. Therefore, the lifetimes obtained as a trace of the $\mathbf{Q}$ matrix are the *total* lifetimes associated with formation and decay of the resonances through all open channels. Using these total lifetimes τ_i the *total* decay rates k_i^d can be easily calculated as[31]

$$k_i^d = 4/\tau_i . \tag{24}$$

For us this expression is useful only at energies $E_i<\Delta$ZPE, when only one channel (let us say channel A) is open, so that $k_i^{d_A}=k_i^d=4/\tau_i$, $k_i^{d_B}=0$, and Eq. (19) for κ_i can be used. At energies $E_i>\Delta$ZPE both channels A and B are open, and, in order to understand the isotope effect, we have to split k_i^d onto the channel-specific decay rates, $k_i^{d_A}$ and $k_i^{d_B}$. It is, however, obvious that

$$k_i^{d_A}+k_i^{d_B}=k_i^d=4/\tau_i . \tag{25}$$

The problem is better understood if we look at the PES for ozone, and imagine the ozone formation process. Several two-dimensional slices of the ozone PES along the hyperradius ρ were shown in our previous paper;[29] here we present a schematic which is a superposition of two slices of the PES: the first slice showing three PES minima (***1***, ***2***, and ***3***) at a small value of $\rho=4$ a.u., where stable O_3 is formed [Fig. 2(a) in Ref. 29], and the second slice showing three asymptotic channels (***A***, ***B***, and ***C***) at a large value of $\rho=14$ a.u., where $O+O_2$ reactants/products are formed [Fig. 3(c) in Ref. 29]. Figure 4 illustrates this schematic of ozone formation when one ^{16}O and two ^{18}O isotopes are involved. In this case the two experimentally undistinguishable $^{18}O+{}^{16}O\,^{18}O$ channels

TABLE I. Positions, lifetimes, channel assignments, and contributions to the total recombination rates of resonances for $^{16}O^{18}O^{18}O$ isotopologue.

	Position of maximum (eV)	Tr **Q** at the maximum (ps)	Background value (ps)	Resonance lifetime (ps)	(%)	Channel	
Below ΔZPE	0.092 185 842 919	54.87	−27.12	82.00	8.79		*A*
	0.092 244 614 178	1764.50	−22.61	1787.11	4.90		*A*
	0.092 363 172 710	5940.30	−16.76	5957.06	2.35		*A*
	0.092 696 312 078	37 204.59	−8.53	37 213.13	0.48		*A*
	0.092 851 921 238	22 651.25	−7.56	22 658.81	0.75		*A*
	0.093 246 889 569	218.40	−4.49	222.89	6.34		*A*
	0.093 263 111 860	1025.38	−4.49	1029.87	4.95		*A*
	0.093 621 618 760	15 969.84	−4.11	15 973.95	0.96		*A*
	0.093 729 058 313	142 853.45	−3.36	142 856.81	0.12		*A*
	0.093 737 992 752	208.86	−29.95	238.81	5.57		*A*
	0.093 840 679 815	734.87	−22.75	757.63	4.70		*A*
	0.093 985 099 738	3496.78	−17.24	3514.02	2.68		*A*
	0.094 017 262 367	1131.05	−16.20	1147.25	4.11		*A*
	0.094 192 793 343	880.46	−11.83	892.29	4.20		*A*
	0.094 466 682 735	144.24	−7.77	152.02	4.74		*A*
	0.094 556 754 507	1150.44	−7.15	1157.58	3.66		*A*
	0.094 632 834 851	27 441.95	−6.32	27 448.27	0.56		*A*
Above ΔZPE	0.094 923 881 122	18.99	−14.98	33.97	2.68	0.83	0.17
	0.094 968 368 504	3630.27	−12.21	3642.48	1.53	0.71	0.29
	0.095 190 240 080	16.74	−27.54	44.28	2.18	*B*	
	0.095 606 000 000	12.96	−4.84	17.80	3.62		*A*
	0.095 656 511 870	86.85	−44.69	131.55	1.89	*B*	
	0.095 684 360 620	41.05	−43.13	84.18	1.89	*B*	
	0.096 146 746 540	171.43	−19.65	191.08	2.46	0.41	0.59
	0.096 460 577 175	69.99	−15.18	85.17	1.54	*B*	
	0.096 633 110 750	58.12	−13.26	71.38	2.73		*A*
	0.096 669 178 601	222.06	−59.34	281.40	1.41	*B*	
	0.096 860 167 374	536.33	−43.28	579.62	2.29	0.08	0.92
	0.097 331 280 754	46.64	−23.48	70.12	1.23	*B*	
	0.097 472 239 173	20.33	−22.84	43.17	1.18	*B*	
	0.098 002 535 592	86.27	−18.37	104.64	1.02	*B*	
	0.098 338 000 000	−22.70	−29.10	6.40	1.74		*A*
	0.098 674 941 270	−3.78	−19.01	15.23	0.86	*B*	
	0.098 867 670 511	25.46	−17.73	43.19	0.81	*B*	
	0.099 219 245 429	−3.17	−16.45	13.29	0.74	*B*	
	0.099 731 734 333	76.58	−30.09	106.67	0.64	*B*	
	0.099 843 539 404	252.74	−28.32	281.06	1.05	0.17	0.83
	0.100 557 000 00	−9.35	−15.38	6.03	0.52	*B*	
	0.100 728 337 11	227.67	−20.68	248.35	0.89	0.02	0.98
	0.100 972 000 00	−18.09	−19.94	1.85	0.86		*A*
	0.101 614 982 69	17.73	−14.54	32.27	0.39	*B*	
	0.102 341 036 10	−2.35	−20.68	18.34	0.32	*B*	
	0.102 451 371 44	−3.20	−19.72	16.51	0.58		*A*
	0.102 620 907 72	49.35	−19.47	68.82	0.31	0.93	0.07
	0.103 110 009 69	38.88	−17.78	56.66	0.26	*B*	
	0.103 170 000 00	−11.25	−12.51	1.26	0.48		*A*
	0.104 041 667 17	176.97	−24.54	201.50	0.21	0.98	0.02
	0.104 286 121 30	−17.57	−23.45	5.88	0.19	*B*	
	0.104 792 878 42	39.70	−20.61	60.32	0.29	0.15	0.85
	0.105 438 230 59	364.00	−18.51	382.51	0.16	0.79	0.21
	0.105 943 894 09	0.46	−17.43	17.90	0.12	*B*	
	0.106 138 081 20	52.30	−17.16	69.46	0.21		*A*
	0.106 405 500 52	6.90	−16.57	23.47	0.14	0.66	0.34
	0.106 729 211 50	−3.57	−26.29	22.73	0.10	*B*	
	0.106 927 653 03	17.62	−25.55	43.18	0.09	*B*	
	0.107 401 689 90	−21.61	−24.00	2.39	0.08	*B*	
	0.108 021 000 00	−18.25	−21.80	3.55	0.13		*A*
	0.108 333 330 68	189.77	−20.81	210.58	0.06	*B*	
	0.109 712 954 40	17.74	−16.64	34.38	0.04	*B*	
	0.110 054 788 25	−5.13	−20.48	15.35	0.04	*B*	
	0.110 747 407 19	−14.40	−18.84	4.45	0.06	0.22	0.78
	0.112 181 151 09	5.48	−15.16	20.64	0.03	0.58	0.42
	0.112 469 857 41	−1.17	−14.84	13.67	0.04		*A*

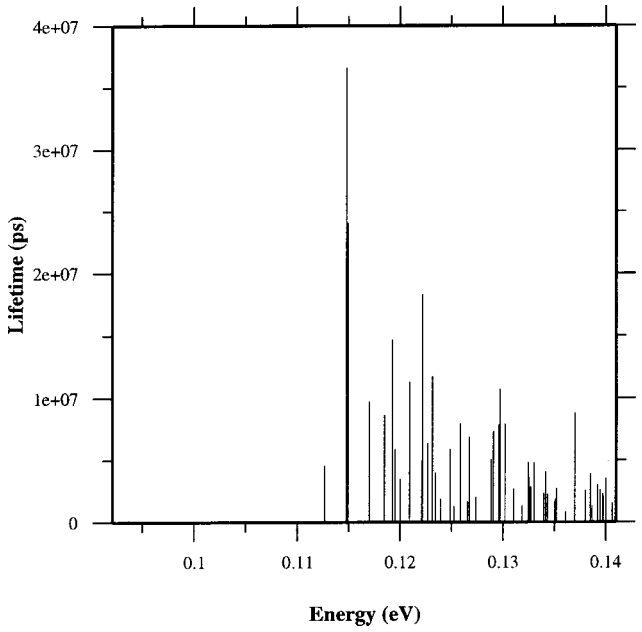

FIG. 2. Same as in Fig. 1 but in a different lifetime scale. Fifty very long-lived resonances with lifetimes in the microsecond range are clearly seen.

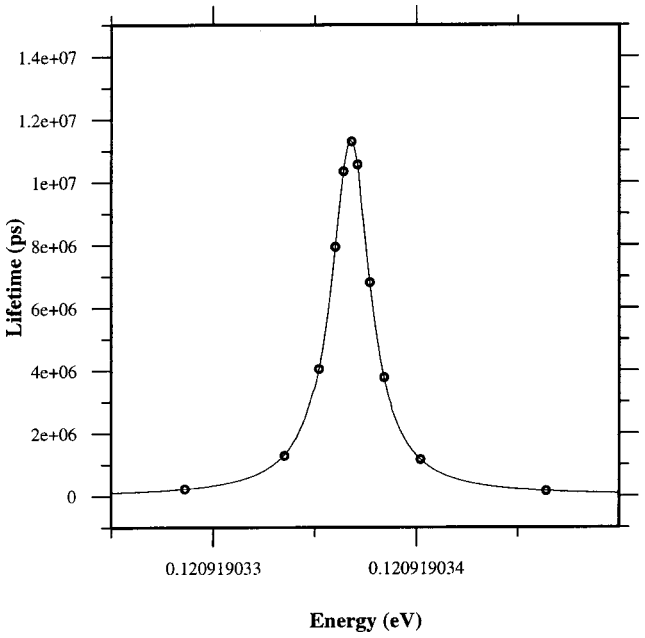

FIG. 3. An example of a very long-lived resonance for $^{16}O\,^{18}O\,^{18}O$ isotopologue. Dots are calculated points; solid line is interpolation using rational function.

(channels ***B*** and ***C***) and one $^{16}O+{}^{18}O\,^{18}O$ channel (channel ***A***) are present. Potential well ***3*** accommodates the symmetric isotopomer $^{18}O\,^{16}O\,^{18}O$, while wells ***1*** and ***2*** accommodate the undistinguishable asymmetric isotopomers $^{16}O\,^{18}O\,^{18}O$. Two distinguishable channels and two distinguishable isotopomers give rise to four experimentally distinguishable formation pathways:

$$
\begin{array}{ccc}
 & {}^{16}O{}^{18}O{}^{18}O & \\
\nearrow & & \nwarrow \\
{}^{18}O + {}^{16}O{}^{18}O & & {}^{16}O + {}^{18}O{}^{18}O \\
\searrow & & \swarrow \\
 & {}^{18}O{}^{16}O{}^{18}O &
\end{array}
\tag{26}
$$

For example, a pathway $^{16}O+{}^{18}O\,^{18}O\rightarrow{}^{18}O\,^{16}O\,^{18}O$, called *insertion*, corresponds to reactants entering interaction region from the channel *A* and forming a metastable state above the well ***3*** (see Fig. 4). Or, a pathway $^{16}O\,^{18}O+{}^{18}O\rightarrow{}^{16}O\,^{18}O\,^{18}O$, called the *end-on process*, corresponds to reactants entering the interaction region from indistinguishable channels *B* or *C* and forming a metastable state above the indistinguishable wells ***1*** and ***2*** (see Fig. 4), and so on.

In the previous paper[29] we used an approximate propagation scheme to obtain and analyze the wave functions for metastable states. A wave function for one long-lived metastable state in the ΔZPE region was presented. It was shown very clearly (see Fig. 9 in Ref. 29) that this metastable state contributes almost exclusively to formation of the symmetric isotopomer $^{18}O\,^{16}O\,^{18}O$ in well ***3***. Furthermore, from the fact that only one $^{16}O+{}^{18}O\,^{18}O$ channel (channel *A*) is open at energies below the ΔZPE we were able to conclude that the metastable state considered contributes almost exclusively to the insertion pathway $^{16}O+{}^{18}O\,^{18}O\rightarrow{}^{18}O\,^{16}O\,^{18}O$. However, an arbitrary chosen metastable $O_3^*(E_i)$ state can have non-zero probability in both $^{18}O\,^{16}O\,^{18}O$ and $^{16}O\,^{18}O\,^{18}O$ wells simultaneously, and can be connected to both $^{16}O+{}^{18}O\,^{18}O$ and $^{18}O+{}^{16}O\,^{18}O$ channels, so that it can contribute to all four pathways of recombination! Corresponding contributions to formation of each isotopomer ($^{18}O\,^{16}O\,^{18}O$ vs $^{16}O\,^{18}O\,^{18}O$) can, in principle, be determined by integrating the wave function of the metastable state over each of the potential wells to determine corresponding probabilities. At

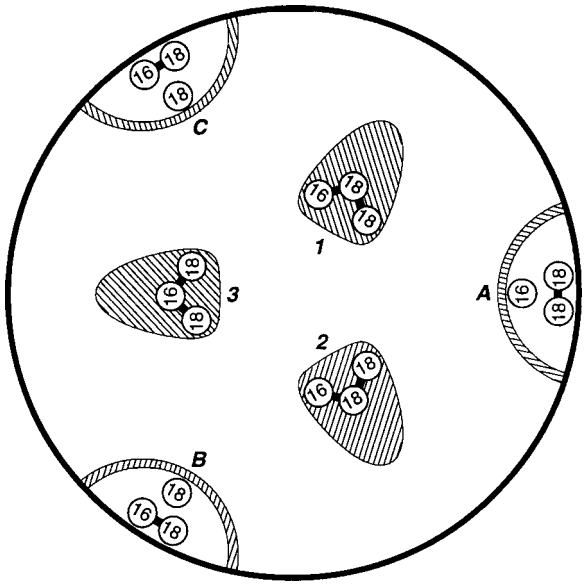

FIG. 4. Schematic of $^{16}O\,^{18}O\,^{18}O$ isotopologue formation. Two slices of the PES are superimposed: the first slice showing three equilibrium wells (***1***, ***2***, and ***3***) and the second slice showing three asymptotic channels (***A***, ***B***, and ***C***). Three isotopomers of ozone are shown in appropriate wells and three reactant pairs are shown in appropriate channels.

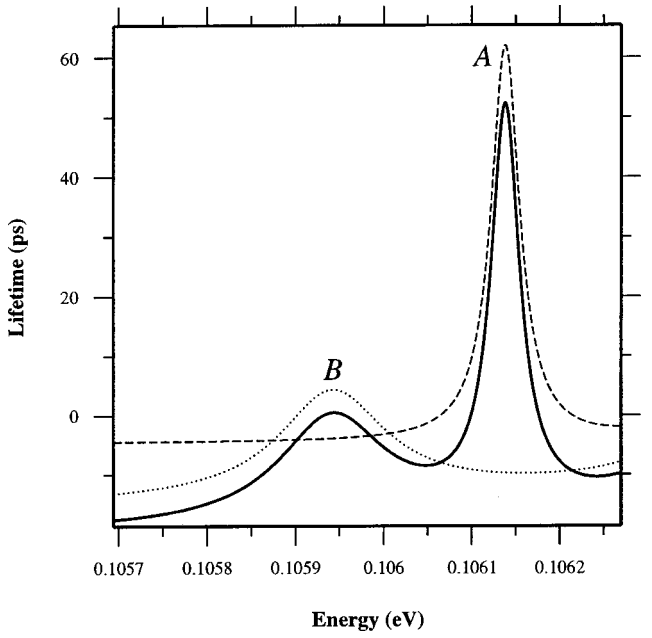

FIG. 5. Example 1. Solid line—a piece of Tr{**Q**} lifetime spectrum for $^{16}O\,^{18}O\,^{18}O$ isotopologue showing two resonances. Dashed line—Tr{$\mathbf{Q}^A$}, dotted line—Tr{$\mathbf{Q}^B$}.

the moment we can not do this, because the accurate propagation technique used in the present work gives the log-derivative of the wave function, rather then the wave function itself. Therefore, in this paper, we chose not to attempt splitting the recombination rate between the two possible isotopomers, i.e., we will consider the overall recombination rate for each channel:

$$^{18}O+{}^{16}O\,^{18}O\rightarrow\left\{\begin{array}{c}{}^{16}O\,^{18}O\,^{18}O\\ \text{.and.}\\ {}^{18}O\,^{16}O\,^{18}O\end{array}\right\}\leftarrow{}^{16}O+{}^{18}O\,^{18}O. \tag{27}$$

From now on, we will call *channel A* a channel containing a symmetric diatomic ($^{16}O+{}^{18}O\,^{18}O$) and *channel B* a channel containing an asymmetric diatomic ($^{18}O+{}^{16}O\,^{18}O$).

To split the decay rate coefficient between the two channels as in Eq. (25), we have to analyze the **Q** matrix in a different way, rather than just calculating its trace. Indeed, elements of our state-to-state **S** matrix for $O+O_2$ collisions are labeled by channels (A or B) and rotational quantum numbers j of O_2 diatomic. Consequently, the elements of the **Q** matrix computed according to Eq. (23) are also labeled by channels and j states of O_2: }

$$\mathbf{Q}=\left(\begin{array}{c|c}m\times m & m\times(n-m)\\ \hline (n-m)\times m & (n-m)\times(n-m)\end{array}\right)\begin{array}{l}\}A\\ \}B\end{array}\qquad \begin{array}{cc}A & B\end{array} \tag{28}$$

Here n is a total number of states in the **S** and **Q** matrixes, m and $(n-m)$ are numbers of states in channels A and B, respectively. Diagonalization of the **Q** matrix mixes channels and states, so that the diagonal form of **Q** has no labels associated with asymptotic states. Eigenvectors, however, are still labeled by channels and j states:

$$\mathbf{Q}=\begin{pmatrix} t_1 & & & & & & \\ & t_2 & & & & & \\ & & t_3 & & & & \\ & & & \ddots & & & \\ & & & & t_k & & \\ & & & & & \ddots & \\ & & & & & & t_n \end{pmatrix},$$

$$\mathbf{u}_k=\begin{pmatrix} u_1 \\ \vdots \\ u_m \\ u_{m+1} \\ \vdots \\ \vdots \\ u_n \end{pmatrix}\begin{array}{l}\}A\\ \\ \\ \}B.\end{array} \tag{29}$$

Eigenvectors are unitary vectors and each satisfies

$$\sum_{l=1}^{n}|u_l|^2=1=\sum_{l=1}^{m}|u_l|^2+\sum_{l=m+1}^{n}|u_l|^2=\alpha^A+\alpha^B. \tag{30}$$

Here α^A and α^B are channel probabilities of t_k. This allows us to split each eigenvalue t_k onto two pieces, proportional to channel probabilities: $t_k=t_k^A+t_k^B$, where $t_k^A=t_k\alpha^A$ and $t_k^B=t_k\alpha^B$. Thus, we have:

$$\mathbf{Q}=\begin{pmatrix} t_1^A+t_1^B & & & & & & \\ & t_2^A+t_2^B & & & & & \\ & & t_3^A+t_3^B & & & & \\ & & & \ddots & & & \\ & & & & t_k^A+t_k^B & & \\ & & & & & \ddots & \\ & & & & & & t_n^A+t_n^B \end{pmatrix}. \tag{31}$$

This allows splitting the trace of **Q** onto two pieces:

$$\mathrm{Tr}\{\mathbf{Q}\}=\sum_{k=1}^{n}t_k=\sum_{k=1}^{n}t_k^A+t_k^B$$

$$=\sum_{k=1}^{n}t_k^A+\sum_{k=1}^{n}t_k^B=\mathrm{Tr}\{\mathbf{Q}^A\}+\mathrm{Tr}\{\mathbf{Q}^B\}. \tag{32}$$

Together with the total lifetime spectrum Tr{**Q**} we can also plot Tr{$\mathbf{Q}^A$} and Tr{$\mathbf{Q}^B$} as functions of energy E and analyze all three spectra simultaneously to get insight into the connection of resonances to the channels. The piece of spectrum shown in Fig. 5 illustrates a typical situation: Two resonances are seen in a spectrum of Tr{**Q**}. One of them appears also in a spectrum of Tr{$\mathbf{Q}^A$}, but not in a spectrum

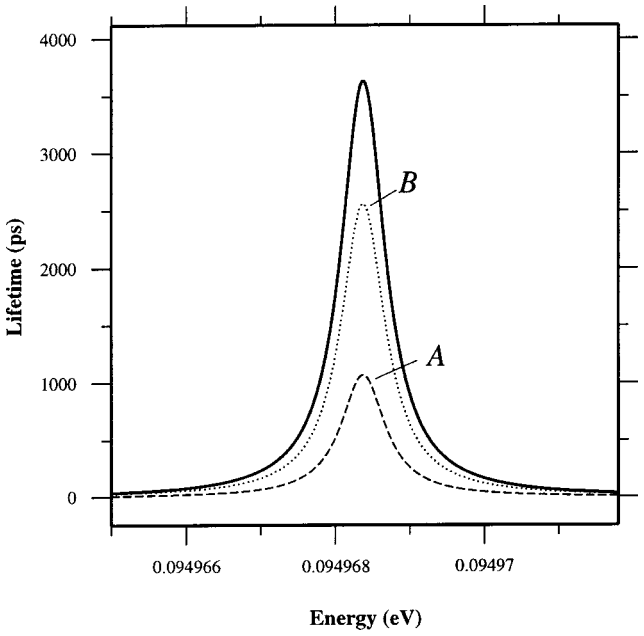

FIG. 6. Example 2. Solid line—a piece of Tr{**Q**} lifetime spectrum for $^{16}O\,^{18}O\,^{18}O$ isotopologue showing one resonance. Dashed line—Tr{$\mathbf{Q}^A$}, dotted line—Tr{$\mathbf{Q}^B$}.

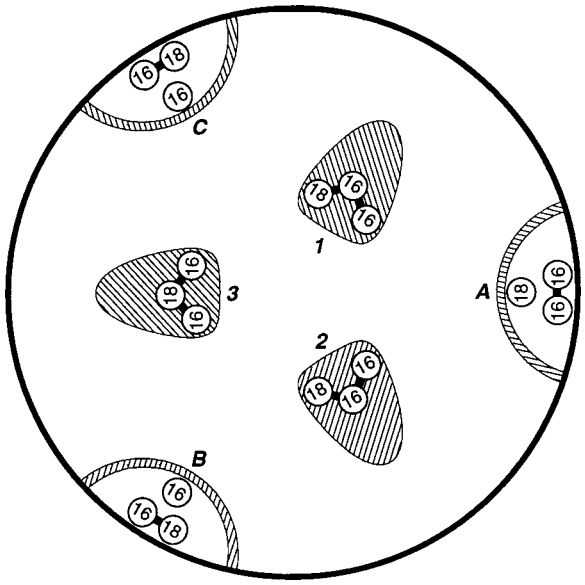

FIG. 7. Same as Fig. 4 but for formation of $^{16}O\,^{16}O\,^{18}O$ isotopologue.

of Tr{$\mathbf{Q}^B$}, i.e., this resonance is associated exclusively with the $^{16}O+^{18}O\,^{18}O$ channel. In contrast, the second resonance appears in a spectrum of Tr{$\mathbf{Q}^B$}, but not of Tr{$\mathbf{Q}^A$}, i.e., it is associated exclusively with the $^{18}O+^{16}O\,^{18}O$ channel. We have found that most of the resonances are associated to only one particular channel and those assignments are given in the last column of Table I. There are, however, cases when the resonance is associated with both channels simultaneously. One example is shown in Fig. 6, where one can clearly see that the contribution of each channel is significant. In Table I, coefficients are given for each such resonance to show its relative participation in each channel. (In addition, simultaneous analysis of Tr{**Q**}, Tr{$\mathbf{Q}^A$}, and Tr{$\mathbf{Q}^B$} allowed us to identify several broad resonances missed previously by analyzing of the Tr{**Q**} alone.)

Before considering the channel-specific recombination rate coefficients and associated isotope effect (Sec. IV), we would like to understand quantitatively the influence of the *positions* and *lifetimes* of $O_3^*(E_i)$ resonances on the recombination process. In the fifth column of Table I we give for each metastable state $O_3^*(E_i)$ its contribution to the overall recombination process calculated as

$$(\%)_i=\frac{\kappa_i^A+\kappa_i^B}{\kappa^A+\kappa^B}\times 100, \tag{33}$$

using Eqs. (15) and (17) for κ^A and κ^B, and Eqs. (16) and (18) for κ_i^A and κ_i^B. Note that the contribution of very narrow resonances is very small: the narrowest resonance in the ΔZPE energy range at $E_i\approx 0.093\,729$ eV with lifetime $\tau_i \approx 143\,853$ ps contributes just 0.12%. This happens because very narrow resonances not only *decay* slowly, but also they *form* so slowly that they never build up a significant concentration and thus cannot contribute much to the recombination rate. One also sees very clearly that contributions of low energy resonances are most important, while the resonances at energies $E_i>110$ K have little effect (about 2%). The reason is that the energy transfer in the stabilization step (7) is rather small ($\Delta E=35$ cm^{-1}) so that only low lying resonances are efficiently stabilized. Both these factors make it very clear that the contribution of resonances at $E_i>240$ K with very long lifetimes in the microsecond range is negligible.

Similar to Fig. 4, Fig. 7 illustrates the scheme of ozone formation when one ^{18}O and two ^{16}O isotopes are involved. In this case four experimentally distinguishable formation pathways are:

$$\begin{array}{ccc} & {}^{16}O\,{}^{16}O\,{}^{18}O & \\ \nearrow & & \nwarrow \\ {}^{16}O+{}^{16}O\,{}^{18}O & & {}^{16}O\,{}^{16}O+{}^{18}O, \\ \searrow & & \swarrow \\ & {}^{16}O\,{}^{18}O\,{}^{16}O & \end{array} \tag{34}$$

while channel-specific recombination rates will reflect just:

$$^{16}O+{}^{16}O\,{}^{18}O\rightarrow\left\{\begin{array}{c}{}^{16}O\,{}^{16}O\,{}^{18}O\\ .\text{and.}\\ {}^{16}O\,{}^{18}O\,{}^{16}O\end{array}\right\}\leftarrow{}^{16}O\,{}^{16}O+{}^{18}O. \tag{35}$$

The calculated spectrum of metastable states for $^{16}O\,^{16}O\,^{18}O$ isotopologue possesses those same features as we have just presented for $^{16}O\,^{18}O\,^{18}O$ isotopologue. The positions, lifetimes, channel assignments, and total contributions of resonances for $^{16}O\,^{16}O\,^{18}O$ are given in Table II in the important energy range $E_i<110$ K.

IV. ANOMALOUS ISOTOPE EFFECT

Here we give a clear explanation of the anomalously large differences in rates for two possible channels forming ozone molecules. Figure 8 shows a schematic for formation of ozone isotopologue $^{16}O\,^{18}O\,^{18}O$. There are two entrance

TABLE II. Positions, lifetimes, channel assignments, and contributions to the total recombination rates of resonances for $^{16}O^{16}O^{18}O$ isotopologue.

	Position of maximum (eV)	Tr **Q** at the maximum (ps)	Background value (ps)	Resonance lifetime (ps)	(%)	Channel	
Below ΔZPE	0.094 676 679 511	−11.01	−29.59	18.59	5.51	*B*	
	0.094 973 588 219	143.51	−9.62	153.14	4.81	*B*	
	0.095 098 011 781	339.28	−24.64	363.92	4.29	*B*	
	0.095 203 220 593	2575.48	−20.13	2595.61	2.31	*B*	
	0.095 378 524 211	42.66	−15.07	57.74	4.50	*B*	
	0.095 414 001 232	44.59	−13.84	58.44	4.46	*B*	
	0.095 480 260 653	882.28	−12.86	895.14	3.31	*B*	
	0.095 669 895 552	25.35	−25.65	51.00	4.18	*B*	
	0.095 800 394 724	981.41	−22.54	1003.95	3.00	*B*	
	0.095 903 645 314	24.09	−20.91	45.00	3.93	*B*	
	0.096 030 058 735	4024.95	−19.04	4043.99	1.60	*B*	
	0.096 283 149 739	14.10	−12.97	27.08	3.58	*B*	
	0.096 436 903 430	139.60	−10.26	149.86	3.31	*B*	
	0.096 638 156 661	101.21	−7.84	109.05	3.18	*B*	
	0.096 680 636 260	365.27	−31.17	396.45	2.90	*B*	
	0.096 805 313 511	17 397.71	−28.87	17 426.58	0.52	*B*	
	0.097 116 769 975	6167.35	−20.02	6187.37	1.08	*B*	
	0.097 533 441 509	32.19	−11.42	43.61	2.55	*B*	
	0.097 567 521 740	9214.95	−10.98	9225.94	0.79	*B*	
	0.097 736 301 128	95.96	−8.72	104.68	2.38	*B*	
Above ΔZPE	0.097 790 600 000	−28.06	−32.08	4.02	5.19		*A*
	0.098 046 334 509	28.97	−41.15	70.12	2.21	*B*	
	0.098 397 717 036	17.48	−25.81	43.29	4.38		*A*
	0.098 851 032 000	−5.88	−12.71	6.83	3.90		*A*
	0.098 948 259 629	1.08	−11.32	12.40	1.76	*B*	
	0.099 151 073 591	218.06	−8.14	226.21	1.61	*B*	
	0.099 380 542 911	17.10	−4.25	21.35	1.56	*B*	
	0.099 474 685 043	23.84	−2.66	26.50	3.29		*A*
	0.099 773 678 034	−1.09	−38.41	37.32	1.40	*B*	
	0.100 595 804 29	27.58	−19.97	47.56	2.43		*A*
	0.100 826 470 27	−10.38	−18.11	7.73	1.06	*B*	
	0.101 104 422 86	−7.18	−16.94	9.76	0.99	*B*	
	0.101 741 087 93	29.04	−23.34	52.37	0.83	*B*	
	0.102 027 114 01	301.32	−21.07	322.38	1.47	0.17	0.83
	0.102 391 272 94	5.55	−18.25	23.80	1.50		*A*
	0.102 568 987 64	1.06	−17.87	18.93	1.24	0.25	0.75
	0.102 472 864 24	68.26	−17.53	85.79	0.68	*B*	
	0.102 793 927 22	31.64	−31.87	63.51	1.35		*A*
	0.103 380 525 64	96.90	−21.84	118.74	0.56	0.96	0.04
	0.104 148 484 37	170.95	−22.77	193.72	0.44	0.99	0.01

channels: $^{16}O+{}^{18}O\,{}^{18}O$ (channel *A*) on the right-hand side of Fig. 8 and $^{16}O\,{}^{18}O+{}^{18}O$ (channel *B*) on the left-hand side. The experimental relative formation rates (relative to the formation rate of the lightest isotopic combination $^{16}O+{}^{16}O\,{}^{16}O\rightarrow{}^{16}O\,{}^{16}O\,{}^{16}O$, taken as a reference for all other isotopic combinations) for channels *A* and *B* are shown at the top of Fig. 8; those give an experimental value of $(\kappa^A/\kappa^B)_{\exp}\approx 1.56$. The energy difference between the two entrance channels is the ΔZPE for reaction (4). Energies below the scattering threshold (the shaded part of Fig. 8) correspond to stable ozone molecules O_3, while metastable states O_3^* can be formed above the threshold energy (white part of the figure). Stabilization of O_3^* to O_3, reaction (3), is shown schematically by descending arrows. This figure illustrates that metastable states at energies *above* the ΔZPE can be formed from both entrance channels. When these states are stabilized, they contribute to channels *A* and *B*. However, the metastable states at energies *below* the ΔZPE can be formed only from the one (lower) entrance channel, namely, $^{16}O+{}^{18}O\,{}^{18}O$, i.e., from the right-hand side of Fig. 8. When stabilized, they contribute exclusively to the corresponding channel *A*. Thus, the metastable states formed in the ΔZPE energy range can be responsible for the anomalous difference in rates for channels *A* and *B*, because they are associated with only the first of them, and not with the second. Here we would like to note again that it is exactly this region below ΔZPE that has the *dense* spectrum of metastable O_3^* states while the upper part of spectrum is *sparse* (see Fig. 1). The part of the spectrum below ΔZPE is rather narrow, but it accommodates a large number of metastable states, and they lie closest to the energy of stable O_3 (see Fig. 8), so that they are stabilized very efficiently by collisions with M, while most states in the energy region above ΔZPE are stabilized at a slower rate. Indeed, from the resonance lifetimes and channel assignments given for $^{16}O\,{}^{18}O\,{}^{18}O$ isotopologue in Table I we have calculated κ^A and κ^B using Eqs. (15)–(18). At ex-

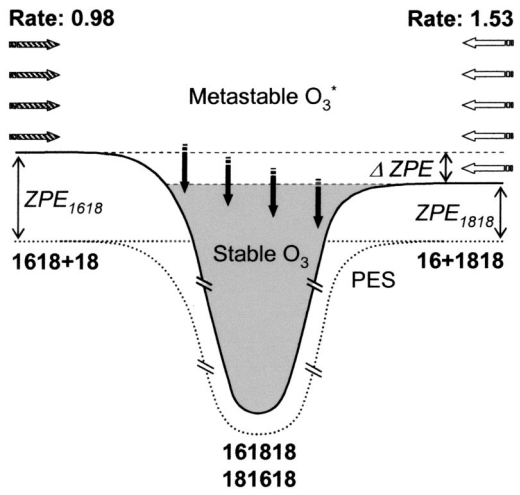

FIG. 8. Schematic for recombination processes forming $^{16}O\,^{18}O\,^{18}O$ isotopologue. The PES (dotted line), the ZPE for two channels, and the ΔZPE are shown (not to scale). Stable ozone molecules are formed in the potential well (shaded part) as a result of collisional stabilization of metastable states formed above the well (in the white part). The stabilization process is shown schematically as black descending arrows. Metastable states above the ΔZPE energy can be formed from both entrance channels: $^{16}O+^{18}O\,^{18}O$ on the right (white arrows) and $^{16}O\,^{18}O+^{18}O$ on the left (striped arrows). Metastable states in the ΔZPE part of spectrum are formed exclusively from the $^{16}O+^{18}O\,^{18}O$ entrance channel. Experimental relative rates of ozone formation for the two channels are given at the top.

perimental conditions of Ref. 9 we found $(\kappa^A/\kappa^B)_{J=0} \approx 3.53$. The *direction* of the isotope effect and its *order of magnitude* are obtained correctly; the absolute value of the effect is about a factor of 2 too large. To explain this difference we recall that our present calculations include only $J=0$ results. We have estimated that J values up to $J=60$ can be important for the recombination process and one should certainly calculate and include them for detailed comparison with the experiment. Later in this section we show that as J increases the isotope effect should decrease, so that the total isotope effect (averaged over all J) should be smaller than the result obtained here for $J=0$ alone.

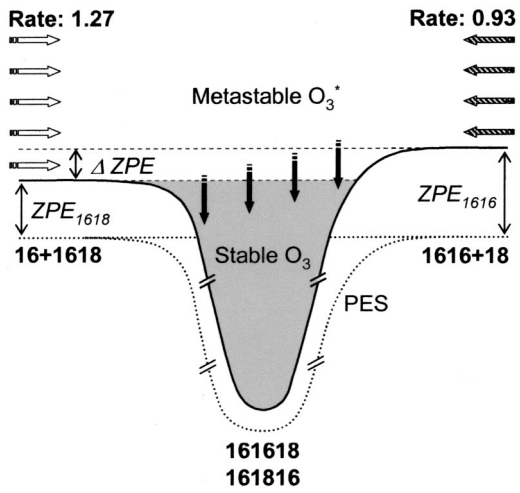

FIG. 9. Same as Fig. 8 but for $^{16}O\,^{16}O\,^{18}O$ isotopologue.

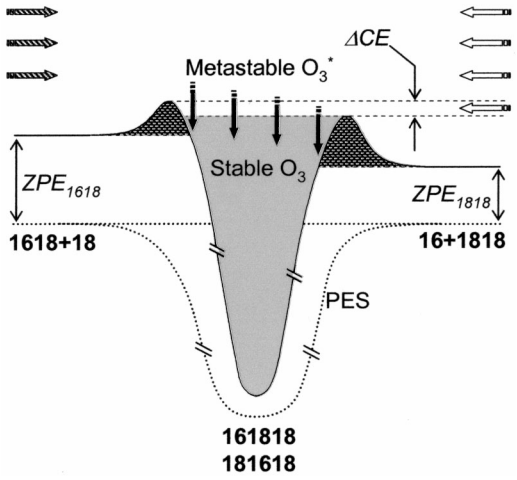

FIG. 10. Effect of $J>0$ on formation of $^{16}O\,^{18}O\,^{18}O$ isotopologue (compare to Fig. 8 for $J=0$). Centrifugal barriers in both channels are shown in black. See the text for discussion of the ΔCE part of the spectrum.

A very similar scheme can be plotted for formation of the $^{16}O\,^{16}O\,^{18}O$ isotopologue (see Fig. 9), but now the lower entrance channel is $^{16}O+^{16}O\,^{18}O$ (channel B) on the left-hand side and the upper channel is $^{18}O+^{16}O\,^{16}O$ (channel A) on the right-hand side. The metastable states in the ΔZPE region can be populated only from the first of them and they contribute exclusively to the rate of channel B. From the experiment[9] $(\kappa^A/\kappa^B)_{\text{exp}} \approx 0.73$. Our theoretical value calculated using resonance lifetimes and channel assignments given for $^{16}O\,^{16}O\,^{18}O$ isotopologue in Table II and Eqs. (15)–(18) is $(\kappa^A/\kappa^B)_{J=0} \approx 0.33$. Again, the *direction* of the isotope effect and its *order of magnitude* are obtained correctly; the absolute value of the effect obtained for $J=0$ is about a factor of 2 larger than experimental.

In the calculations at total $J>0$ we expect to see a new effect associated with the appearance of centrifugal barriers. A rising centrifugal barrier can prevent population of resonances in the ΔZPE part of the spectrum, because oxygen atoms are heavy, and tunneling through the barrier is slow. For example, one can ask the question: At what value of J will the centrifugal barrier in the lower entrance channel rise up to the level of ΔZPE? A simple estimate gives value of $J=19$ for $^{16}O\,^{18}O\,^{18}O$ isotologues. So, one can expect that at $J>19$ there will be no active metastable states in the ΔZPE energy region. However, while the centrifugal barrier in the lower channel rises (as J increases) and shields the ΔZPE part, the centrifugal barrier in the upper channel also rises and now a part of the spectrum between the centrifugal barriers in the lower and upper channels (ΔCE—*delta-centrifugal-energy*) may play the same role at larger J that the ΔZPE part of the spectrum plays at $J=0$. We expect that at $J>0$ the dense part of the spectrum can be found in the ΔCE energy range (see the schematic in Fig. 10). It is also interesting that the centrifugal barrier in the lower channel rises faster than the barrier in the upper channel due to the difference in the effective masses μ_A and μ_B, and one can ask the following question: At what value of J will the centrifugal barriers on the left- and right-hand sides of Fig. 10 become equal? A simple estimate gives a value of $J=31$ for

$^{16}O\,^{18}O\,^{18}O$ isotopologue. We expect that at this value of J the dense part of the resonance spectrum will disappear, because now all channels contain barriers at equal energies ($\Delta CE=0$). Further increase of J will cause further increase of the centrifugal barriers, but now the barrier in the lower channel will be higher than the barrier in the upper channel and the isotope effect can clearly go in the reverse direction! Our estimates show that at room temperature $0<J<60$ can contribute to the formation of the resonances in reaction (2). These simple ideas show how complex the effect of $J>0$ can be. It certainly requires additional theoretical consideration and will be reported later.

Anomalous differences in recombination rates are due to the many metastable states in the ΔZPE part of the spectrum. The ZPE itself is a quantum mechanical entity not present in classical mechanics. It is now easy to understand why classical mechanics studies cannot explain the effect. Indeed, a classical trajectory is allowed to access the very bottom of the potential well (the lower dotted curve in Figs. 8 and 9) and it is the same on both sides of reaction (4) independent of the isotopic composition (x,y,z). In contrast, the quantum mechanical states start not from the bottom of the PES, but from ZPE and the ZPE is different for $^{y}O\,^{z}O$ on the left- and $^{x}O\,^{y}O$ on the right-hand sides of reaction (4). This also suggests that this isotope effect is a quite general quantum mechanical effect and should be seen in other homonuclear triatomic molecules supporting an important number of metastable states within the ΔZPE energy range.

In relation to this we want to mention that the potential energy curve for a general atom-exchange reaction,

$$A+BC\Leftrightarrow(ABC)^{*}\Leftrightarrow AB+C, \tag{36}$$

easily found in almost any textbook on chemical reactivity, is somewhat similar to the solid curve in Figs. 8 and 9. Nevertheless its meaning is very different. In a textbook case the energy difference between A+BC and AB+C channels is due to the difference in formation energies of BC and AB molecules. These molecules are different chemical species with different electronic structures. But in the case of ozone the $^{y}O\,^{z}O$ and $^{x}O\,^{y}O$ diatomics are the same chemical species having the same electronic structure and differ only by the ZPE of their quantum rovibrational states. It also means that the standard reaction (36) should be treated with caution, because for some systems the ΔZPE can be important and cause isotope effects similar to that found in ozone.

V. CONCLUSIONS

The kinetics of the ozone formation was studied by considering the three-body recombination reaction $O+O_2+M\rightarrow O_3+M$. In the energy-transfer mechanism, the metastable state of ozone O_3^{*} is formed first in a two-body $O+O_2$ collision and then stabilized to O_3 by a collision with third body M. A sophisticated treatment was employed, which considers different metastable $O_3^{*}(E_i)$ states as different species; their lifetimes were obtained from full dimensional quantum scattering studies using a coupled-channel approach and hyperspherical coordinates on an accurate *ab initio* potential energy surface.

Different isotopologues of ozone were considered with a view toward understanding the anomalous isotope effect of ozone formation. It was found that the lifetime spectra of metastable O_3^{*} states exhibit a pronounced nonstatistical feature: there are many long-lived metastable states within the narrow ΔZPE energy range, and there are only few metastable states at energies above the ΔZPE. It was quantitatively shown that this feature of metastable states is responsible for the anomalous isotope effect in ozone formation. The metastable states at energies below the ΔZPE are accessible only from the lower entrance channel. These low-lying metastable states can be stabilized very efficiently (by collisions with third bodies M) because they are energetically close to the bound O_3 states. Such processes enhance significantly the formation rates of ozone isotopologues through the lower channels ($^{16}O+^{18}O\,^{18}O$ and $^{16}O+^{16}O\,^{18}O$) over the formation rates through the upper channels ($^{16}O\,^{18}O+^{18}O$ and $^{16}O\,^{16}O+^{18}O$, respectively).

Numerical calculations of the recombination rates at $J=0$ give the isotope effects in the right direction and of the right order of magnitude. Calculated absolute values of the isotope effects at $J=0$ are about twice larger than experimental values, where a broad distribution of angular momentum states contributes. We have qualitatively shown that at $J>0$ the isotope effect should decrease, because the ΔZPE part of spectrum becomes narrower and will be able to accommodate fewer resonant states. Therefore, including $J>0$ states into consideration should improve comparison of the theory and experiment. These calculations are under way and will be reported later.

In addition to the quantitative description offered in this paper, several qualitative conclusions can also be made about the isotope effects in ozone formation. For example, we can clearly see now why two possible insertion pathways exhibit very different experimental[9] rates: $^{16}O+^{18}O\,^{18}O\rightarrow{}^{18}O\,^{16}O\,^{18}O$ has relative rate of 0.029, while $^{18}O+^{16}O\,^{16}O\rightarrow{}^{16}O\,^{18}O\,^{16}O$ has relative rate of 0.006. The first reaction proceeds through the lower channel and can enter below the ΔZPE threshold (see Figs. 4 and 8), while the second reaction proceeds through the upper channel and enters the interaction region only at energies above the ΔZPE (see Figs. 7 and 9). Participation of the resonances below the ΔZPE and easier stabilization of these low energy resonances by third-body collisions makes the first of these insertion reactions much faster than the second one.

It is also understood now why the isotope effect on the relative reaction rates becomes larger as temperature decreases.[42] At lower temperatures the population of the lower parts of the O_3^{*} spectrum increases and the contribution of the ΔZPE part becomes more important relative to the contribution of the higher energy part. [Strictly speaking, if the energy of the reagents in reaction (4) drops below the ΔZPE, then the forward direction of the atom exchange reaction (4) is energetically closed.] However, studying the temperature dependence of the isotope effect theoretically requires more knowledge about the stabilization step (3). Namely, the temperature dependence of the stabilization en-

ergy transfer $\Delta E(T)$ should be calculated quantum mechanically, or some sophisticated model should be used to describe it.

ACKNOWLEDGMENTS

This work was performed under the auspices of the U.S. Department of Energy (under Contract No. W-7405-ENG-36). D.B. acknowledges the Laboratory Directed Research and Development program in Los Alamos for granting a Postdoctoral Fellowship. This research used resources of the National Energy Research Scientific Computing Center, which is supported by the Office of Science of the U.S. Department of Energy under Contract No. DE-AC03-76SF00098. We acknowledge Professor Konrad Mauersberger and his group at Heidelberg for helpful discussions on anomalous isotope effects in ozone formation.

[1] K. Mauersberger, Geophys. Res. Lett. **8**, 935 (1981).
[2] M. H. Thiemens and J. E. Heidenreich III, Science **219**, 1073 (1983).
[3] M. H. Thiemens, Science **283**, 341 (1999).
[4] K. Mauersberger, B. Erbacher, D. Krankowsky, J. Gunther, and R. Nickel, Science **283**, 370 (1999).
[5] P. Lammerzahl, T. Rockmann, C. A. M. Brenninkmeijer, D. Krankowsky, and K. Mauersberger, Geophys. Res. Lett. **29**, 104013 (2002).
[6] J. Morton, J. Barnes, B. Schueler, and K. Mauersberger, J. Geophys. Res., [Space Phys.] **95**, 901 (1990).
[7] D. Krankowsky and K. Mauersberger, Science **274**, 1324 (1996).
[8] S. M. Anderson, D. Hulsebusch, and K. Mauersberger, J. Chem. Phys. **107**, 5385 (1997).
[9] C. Janssen, J. Guenther, D. Krankowsky, and K. Mauersberger, J. Chem. Phys. **111**, 7179 (1999).
[10] C. Janssen, J. Guenther, D. Krankowsky, and K. Mauersberger, J. Chem. Phys. **112**, 11109 (2000).
[11] S. Wolf, M. Bitter, D. Krankowsky, and K. Mauersberger, J. Chem. Phys. **113**, 2684 (2000).
[12] J. E. Heidenreich III and M. H. Thiemens, J. Chem. Phys. **84**, 2129 (1986).
[13] J. Guenther, D. Krankowsky, and K. Mauersberger, Chem. Phys. Lett. **324**, 31 (2000).
[14] J. A. Kaye and D. F. Strobel, J. Geophys. Res., C: Oceans Atmos. **88**, 8447 (1983); **90**, D7, 7865 (1986).
[15] A. Gross and G. D. Billing, Chem. Phys. **217**, 1 (1997).
[16] D. R. Bates, J. Chem. Phys. **93**, 8739 (1990).
[17] G. Gellene, Science **274**, 1344 (1996).
[18] D. Charlo and D. C. Clary, J. Chem. Phys. **117**, 1660 (2002).
[19] A. Miklavc and S. D. Peyerimhoff, Chem. Phys. Lett. **359**, 55 (2002).
[20] T. A. Baker and G. I. Gellene, J. Chem. Phys. **117**, 7603 (2002).
[21] C. Janssen, J. Guenther, K. Mauersberger, and D. Krankowsky, Phys. Chem. Chem. Phys. **3**, 4718 (2001).
[22] B. C. Hathorn and R. A. Marcus, J. Chem. Phys. **111**, 4087 (1999).
[23] B. C. Hathorn and R. A. Marcus, J. Chem. Phys. **113**, 9497 (2000).
[24] B. C. Hathorn and R. A. Marcus, J. Phys. Chem. A **105**, 5586 (2001).
[25] Y. Q. Gao and R. A. Marcus, Science **293**, 259 (2001).
[26] C. Janssen and R. A. Marcus, Science **294**, 951a (2001).
[27] Y. Q. Gao and R. A. Marcus, J. Chem. Phys. **116**, 137 (2002).
[28] Y. Q. Gao, W.-C. Chen, and R. A. Marcus, J. Chem. Phys. **117**, 1536 (2002).
[29] D. Babikov, B. K. Kendrick, R. B. Walker, P. Fleurat-Lessard, R. Schinke, and R. T Pack, J. Chem. Phys. **118**, 6298 (2003).
[30] D. Babikov, B. K. Kendrick, R. B. Walker, R. Schinke, and R. T Pack, Chem. Phys. Lett. **372**, 686 (2003).
[31] R. T Pack, R. B. Walker, and B. K. Kendrick, J. Chem. Phys. **109**, 6714 (1998).
[32] J. Troe, J. Chem. Phys. **66**, 4745 (1977).
[33] H. Hippler, R. Rahn, and J. Troe, J. Chem. Phys. **93**, 6560 (1990).
[34] R. Siebert, R. Schinke, and M. Bittererova, Phys. Chem. Chem. Phys. **3**, 1795 (2001).
[35] R. Siebert, P. Fleurat-Lessard, M. Bittererova, S. C. Farantos, and R. Schinke, J. Chem. Phys. **116**, 9749 (2002).
[36] P. Fleurat-Lessard, S. Yu. Grebenshchikov, R. Siebert, R. Schinke, and N. Halberstadt, J. Chem. Phys. **118**, 610 (2003).
[37] B. K. Kendrick, R. T Pack, R. B. Walker, and E. F. Hayes, J. Chem. Phys. **110**, 6673 (1999), and references therein.
[38] B. K. Kendrick, J. Chem. Phys. **114**, 8796 (2001).
[39] B. R. Johnson, J. Chem. Phys. **67**, 4086 (1977).
[40] F. Mrugala and D. Secrest, J. Chem. Phys. **78**, 5954 (1983).
[41] F. T. Smith, Phys. Rev. **118**, 349 (1960).
[42] C. Janssen, J. Guenther, D. Krankowsky, and K. Mauersberger, Chem. Phys. Lett. **367**, 34 (2003).